

Spectroscopic and electrochemical analyses of electron transfer and mass transfer across the microdroplet/solution interface

N. Kitamura, K. Nakatani, and H.-B. Kim

Department of Chemistry, Faculty of Science, Hokkaido University,
Sapporo 060, Japan

Abstract - A laser trapping - spectroscopy - electrochemistry method has been applied to study electron transfer and mass transfer across the microdroplet/water interface. Electron transfer from Fe(III) produced electrochemically at an optically transparent SnO₂ electrode in water to ferrocene (FeCp) in an oil droplet was directly measured by both fluorometric and coulometric methods. The rate determining step of the FeCp oxidation was the electron transfer process across the droplet/water interface and the relevant rate constant was determined for individual micrometer droplets. As a model of color developing reactions in photographic emulsions, cyan dye formation reaction in a single oil droplet was also investigated. Mass transfer of a reagent across the droplet/water interface and subsequent dye formation reaction in the droplet were demonstrated. The yield and the rate constant of the dye formation reaction in single droplets were also discussed.

INTRODUCTION

Microchemical techniques capable of investigating reactions proceeding in micrometer small volumes have been developed in recent years (ref. 1, 2). As an example, space- and time-resolved absorption and emission spectroscopy based on an ultrafast laser and an optical microscope were successfully applied to study characteristic features of photochemistry and photophysics in micrometer - picosecond dimensions (ref. 3, 4), and pyrene excimer formation dynamics in individual microcapsules or microdroplets was demonstrated (ref. 5, 6). Recent advances in microfabrication technologies also enabled one to conduct and control electrochemical reactions in micrometer domains by using microelectrodes. In particular, we showed that photochemical and electrochemical control of reactions in micrometer dimensions was possible by the use of semiconductor-based microelectrode arrays (ref. 7). Furthermore, an optical trapping method has been currently introduced for manipulation of very small samples, in which an individual microparticle or substance undergoing Brownian motion in solution can be arbitrarily manipulated in three-dimensional space by a focused infrared laser beam (ref. 8 - 10). Since the optical trapping method provides non-contact and non-destructive manipulation of a single microparticle in solution, a combination of the technique with spectroscopic and electrochemical methods under a microscope is expected to open a new research field of "*chemistry of single microparticles*". It is noteworthy that a non-contact and non-destructive manipulation method for individual microparticles in solution has been unavailable until introducing the optical trapping technique, so that experimental results so far obtained for microparticles are regarded as the sum or average of those for particles with various properties and diameters. Clearly, measurements of a number of particles by space-unresolved methods cannot afford a clear picture of chemistry of microparticles. An optical trapping - spectroscopy - electrochemistry method, which makes it possible to measure single microparticles, will therefore greatly contribute to the understanding of chemical reactions proceeding in individual microparticles or across the particle/ solution boundary.

Among various microparticles, we focused our research attention on micro-oil-droplets in emulsion systems. Our main reason for studying chemical processes in oil-in-water emulsions is their importance in basic research and various industries. For example, understanding of chemistry in single microdroplets dispersed in solution is the fundamental basis for solvent extraction, physical chemistry at the liquid-liquid interface, photographs, foods chemistry, and so forth. Furthermore, oil-in-water or water-in-oil emulsions have been of great interest and extensively studied in the field of photochemistry and photophysics with special reference to achievement of a high charge separation efficiency of redox products in photoinduced electron transfer. Development of an optical trapping - spectroscopy - electrochemistry method for single microparticles and its potential applications will provide an inside look at various chemical phenomena proceeding in individual microdroplets. In this article, we describe the optical trapping - spectroscopy - electrochemistry method and its applications to studying electron transfer and mass transfer across the microdroplet/solution interface.

MICROCHEMICAL METHOD FOR SINGLE PARTICLES

A schematic diagram of an optical trapping - spectroscopy - electrochemistry system is illustrated in Fig. 1. A 1064 nm laser beam from a CW Nd³⁺ : YAG laser was used for an optical trapping light source. The laser beam was introduced to an optical microscope and the beam focused by a microscope objective (~ 1 μm spot) was irradiated to a sample solution set on the microscope stage. When the refractive index of a microparticle (n_1) is different from that of the surrounding medium (n_2), the laser beam refracts at the particle/solution boundary and the light refraction causes a momentum change with the amount of ΔP . The change in light momentum should be conserved, so that the same amount of the momentum change is exerted to the particle with the direction opposite to ΔP ; $-\Delta P$. The sum of $-\Delta P$ generated at the particle/solution boundary irradiated by the laser beam, called as the radiation force, acts as driving force for optical (laser) trapping of the microparticle (ref. 11). Under the condition of $n_1 > n_2$, the radiation force directs to the focal spot of the laser beam and the particle is "trapped" in the vicinity of the focal spot. Even if the laser-beam spot is shifted in the XY plane, the particle follows the laser-beam spot so the particle can be manipulated in the XY plane. Furthermore, although the radiation force is as small as several pico Newtons (pN), gravitational force experienced by a microparticle is much smaller than pN so that a particle is levitated in space by the laser beam, leading to three-dimensional manipulation of an individual microparticle. Actually, we confirmed laser manipulation of polymer beads, oil droplets, glass beads, microcapsules, biological cells, and so forth as reported previously (ref. 8 - 10, 12). At ambient temperature, the Brownian motion of a microparticle in solution is completely suppressed by laser trapping. The optical trapping/manipulation method can be thus applied to selection and characterization of an arbitrary microparticle in solution.

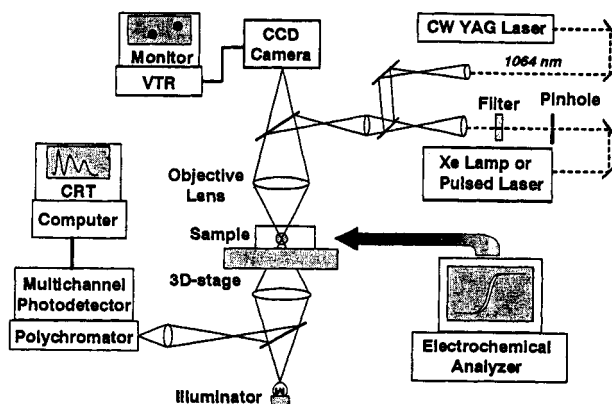


Fig. 1. A block diagram of the laser trapping - spectroscopy - electrochemistry system

With a microparticle in solution being laser-trapped, a light beam from a pulsed laser or other monochromatic light source was introduced to the microscope coaxially with the trapping laser beam to conduct emission or absorption spectroscopy of the laser-trapped particle. Fluorescence from the particle was collected by the objective lens and detected by a photodiode array attached to the microscope. For absorption spectroscopy, transmitted light from the particle was passed through a condenser lens, reflected by a mirror, and introduced to the detector. Both absorption and fluorescence spectra obtained for a single microparticle showed a good S/N ratio even for measurements under an optical microscope. Electrochemical measurements of a single particle were conducted by setting a microelectrode or its array in an electrolytic cell on the microscope stage. A particle was arbitrarily manipulated and positioned *on* or *in the vicinity* of the electrode, and electrochemical reactions of the particle or surrounding solution phase were induced by controlling an electrode potential through an external equipment. Special care was taken to avoid noise from lasers and other light sources to measure a current as small as nano- ~ pico-ampere. Using an optically transparent electrode, both spectroscopic and electrochemical measurements on a single, laser-trapped particle were also conducted. Spectroscopic and electrochemical measurements of a single particle as small as ~10 μm were successful by the laser system in Fig. 1.

ELECTRON TRANSFER ACROSS MICRODROPLET/WATER INTERFACE

For designing and conducting efficient redox reactions in oil-in-water emulsions, the overall reaction mechanisms and the factors influencing its efficiency should be elucidated. Nonetheless, reactions in emulsions are in general very complicated since those involve diffusion of a reactant(s)/product(s) in both water and oil phases and electron/mass transfer across the droplet/water interface. Furthermore, the chemical processes across the droplet/water interface are expected to depend on droplet size, interfacial properties, and so forth. A study on emulsions should be done for individual droplets. As an example, we investigated electron transfer across the microdroplet/water interface based on the optical trapping - spectroscopy - electrochemistry method. The reaction system studied was oxidation of ferrocene (FeCp) by Fe(III) across the micro oil-droplet/water interface, and the time course of the oxidation reaction was monitored simultaneously by spectroscopic and electrochemical methods. A tri-*n*-butylphosphate (TBP) solution containing FeCp (0.1 M) and 9,10-diphenylanthracene (DPA ; 0.01 M) was vigorously mixed with an aqueous solution of $\text{Fe}(\text{CN})_6^{4-}$ (Fe(II) ; 0.2 mM), tetra-*n*-butylammonium chloride (1×10^{-2} M), and MgSO_4 (0.1 M) to prepare TBP microdroplets (diameter (d) = 0.5 ~ 40 μm ; average $d \sim 4 \mu\text{m}$) in water. An aqueous solution of sodium dodecylsulfate (SDS ; 3.0 wt %) was further added to the mixture to stabilize the TBP droplets. As an electrolytic cell, the TBP/water emulsion was placed between an optically transparent SnO_2 electrode (working electrode) and a glass plate. A Pt wire and an Ag/AgCl were used as counter and reference electrodes, respectively.

Before single-droplets measurements were made, we performed experiments for a number of the TBP droplets with the electrolytic cell being immersed in a cuvette containing the emulsion (ref. 13). When a potential (800 mV vs. Ag/AgCl) was applied to the SnO_2 electrode by a controlled potential coulometric method, the current (i) relevant to oxidation of $\text{Fe}(\text{CN})_6^{4-}$ (Fe(II)) to $\text{Fe}(\text{CN})_6^{3-}$ (Fe(III)) in the water phase was observed. One of the important findings was the fact that the total electric charge at the electrode was much larger in the presence of FeCp in the droplets (i_{FeCp}) as compared with that in the absence of FeCp (i_0). This can be easily seen from Fig. 2a that, without FeCp in the droplets, the oxidation of Fe(II) is almost complete within the electrolytic time (t) of ~ 20 s while it continues to $t = 100$ s in the presence of FeCp. It is noteworthy that, although the oxidation potential of FeCp in TBP is 230 mV, FeCp is not oxidized to ferrocenium cation (FeCp^+) without Fe(II) in the water phase at 0 - 800 mV. These results explicitly indicate that FeCp in the droplets is oxidized to FeCp^+ by Fe(III) via electron transfer across the droplet/water interface, and the difference between i_{FeCp} and i_0 corresponds to the total mole number of FeCp in the TBP droplets. The total amount of FeCp is 2.5 times higher than that of Fe(II), so that Fe(II) regenerated by electron transfer with FeCp at the droplet/water interface should be oxidized again to Fe(III)

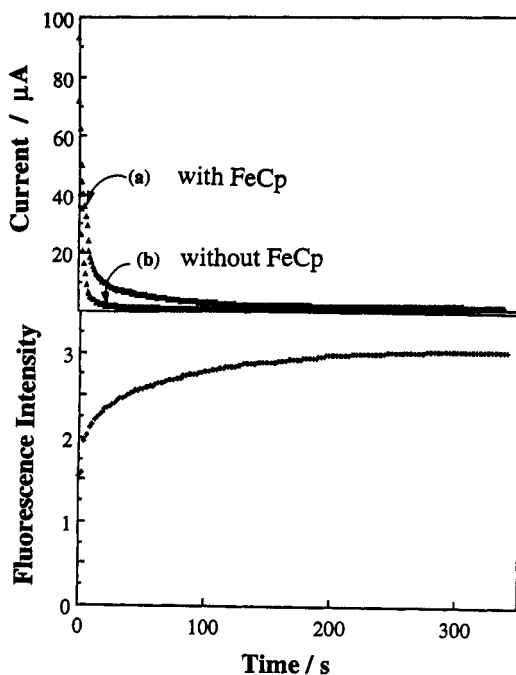


Fig. 2. Time dependences of i (upper trace) at the electrode and I^F from the DPA/TBP droplets (lower trace) during electrolysis of PPD in the water phase.

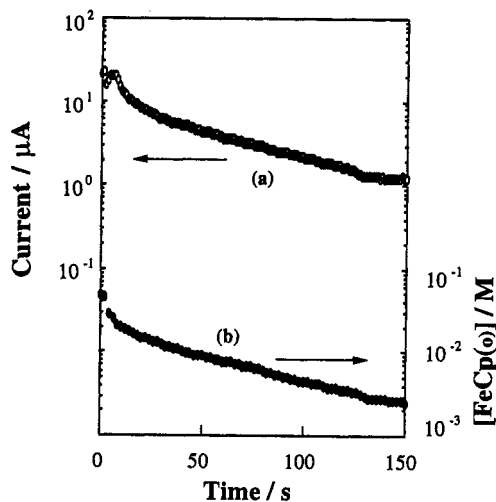
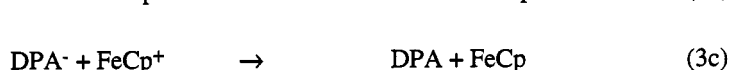
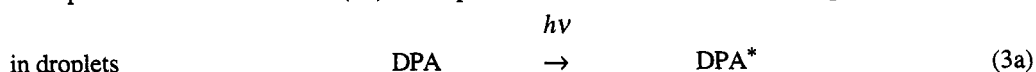
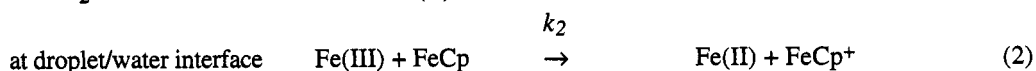
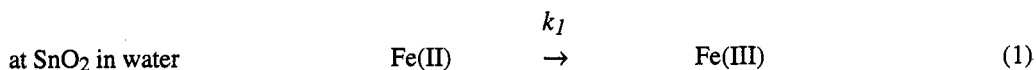


Fig. 3. Time dependences of Δi (a) and $[\text{FeCp}(0)]$ (b) during electrolysis of PPD in the water phase.

at the electrode (i.e., redox cycle) to cause complete oxidation of FeCp in the droplets. On the other hand, the oxidation of FeCp accompanies enhancement of the fluorescence intensity (I^F) of DPA in the TBP droplets (Fig. 2b). In TBP, the excited singlet state of DPA (DPA^*) is quenched by FeCp through electron transfer from FeCp to DPA^* . Therefore, before electrolysis of Fe(II) in the water phase, DPA^* in the droplets is efficiently quenched by FeCp. However, the interfacial electron transfer from Fe(III) to FeCp causes a decrease in the FeCp concentration in the droplets and FeCp^+ does not possess a quenching ability towards DPA^* , so that the fluorescence intensity of DPA increases with the electrolytic time. The time course of I^F thus corresponds to that of the FeCp concentration in the TBP droplets during electrolysis of Fe(II) in the water phase. In the present emulsion system, the reactions are thus supposed to proceed via the following mechanism.



k_1 and k_2 are the rate constants of bulk electrolysis of Fe(II) at the electrode and electron transfer between Fe(III) and FeCp across the droplet/water interface, respectively. k_3 is the rate constant for the electron transfer quenching of DPA* by FeCp in the droplet, and has been determined to be $3.1 \times 10^9 \text{ M}^{-1}\text{s}^{-1}$ by a separate experiment (ref. 13).

According to the above discussions, the curve given by subtracting the $i_0 - t$ curve from the $i_{\text{FeCp}} - t$ data (i.e., $\Delta i - t$) should correspond to a time conversion profile for the oxidation of FeCp in the droplets, and is proportional to the concentration of FeCp in the droplets ($[\text{FeCp}(o)]$), as the $\log \Delta i - t$ curve relevant to the data in Fig. 2 is shown in Fig. 3. The total electric charge calculated by integrating the $\Delta i - t$ curve at $t < 150 \text{ s}$ was $\sim 7 \times 10^4 \text{ C}$. The value agrees very well with the total amount of FeCp in the droplets ($7 \times 10^4 \text{ C}$), indicating that FeCp in the droplets is oxidized via the redox cycles of Fe(II)/Fe(III) in the water phase. Close inspection of Fig. 3a indicates that, although $\log \Delta i$ decreases almost linearly with t , it deviates from the linearity at $t < 20 \text{ s}$. This particular time range corresponds to that of the sharp decrease of i in Fig. 2a. At $t < 20 \text{ s}$, the phenomena seem to be very complicated and therefore we focus our discussion on the results at $t > 20 \text{ s}$.

A Stern - Volmer relation, $I^F/I^F_0 = 1 + k_3\tau_0[\text{FeCp}(o)]$, can be used to calculate $[\text{FeCp}(o)]$ in the droplet on the basis of the observed I^F data, where I^F_0 is I^F for $[\text{FeCp}(o)] = 0$ and assumed to be equal to I^F at $t \sim 300 \text{ s}$. τ_0 is the excited singlet state lifetime of DPA (6.7 ns). Knowing I^F at various t , a time dependence of $\log[\text{FeCp}(o)]$ was calculated as shown in Fig. 3b. The time course of $[\text{FeCp}(o)]$ is very similar to that of Δi at $t > 20 \text{ s}$ and, therefore, the oxidation reaction of FeCp in the droplets can be discussed based on the data in Fig. 3. It is noteworthy that the diffusion time of Fe(II) or Fe(III) (diffusion coefficient ; $D = 7 \times 10^{-6} \text{ cm}^2\text{s}^{-1}$) necessary to pass the electrolytic cell (thickness $\sim 70 \mu\text{m}$) is 3.5 s. Apparently, the value is very short as compared with the observed electrolytic time, indicating that mass transfer of Fe(II) or Fe(III) between the droplets and the electrode is not the rate-determining step for the FeCp oxidation. The very good correspondence between the $\Delta i - t$ and $[\text{FeCp}(o)] - t$ curves also supports for this. It is easily expected, furthermore, that mass transfer of FeCp in the droplet is also very fast because the diameter of the droplet is of the order of micrometer. Therefore, we concluded that the rate-determining step in the present system was the electron transfer between Fe(III) and FeCp across the droplet/water interface. The time profile of Δi or $[\text{FeCp}(o)]$ at $t > 20 \text{ s}$ in Fig. 3 was thus analyzed as a pseudo first-order reaction and k_2 was determined to be $80 \text{ M}^{-1}\text{s}^{-1}$ under the assumption of $[\text{Fe(III)}] = 2.0 \times 10^{-4} \text{ M}$. This corresponds to the rate constant per unit area at the droplet interface, defined as $k_2' = (V/A)k_2$, to be $\sim 5 \times 10^{-3} \text{ M}^{-1}\text{cm}^2\text{s}^{-1}$ for the droplet with $d \sim 4 \mu\text{m}$, where $A = 4\pi(d/2)^2$ and $V = 4/3\pi(d/2)^3$ are the surface area and the volume of the droplet, respectively.

Spectroscopic and electrochemical methods were shown to be successful to determine the rate constant of electron transfer across the droplet/water interface, so that the methods were applied to single-droplet measurements. In the experiments, the electrolytic cell was set on the microscope stage, and a single droplet was levitated in the sample emulsion by the focused 1064 nm laser beam. A change in I^F during electrolysis of Fe(II) in the water phase was then monitored by the microspectroscopic method. The I^F values obtained at various t were converted to $[\text{FeCp}(o)]$ based on the Stern - Volmer relation, and we found that $[\text{FeCp}(o)]$ for a single droplet ($d = 34 \mu\text{m}$) was a linear function of t except for $t < 20 \text{ s}$ analogous to the data in Fig. 3. Similar experiments were performed for various droplets with different diameter. k_2 determined for an individual droplet decreases from ~ 140 to $\sim 20 \text{ M}^{-1}\text{s}^{-1}$ with increasing the diameter of the droplet from 10 to 40 μm . This implies that the smaller the droplet, the shorter the time necessary to oxidize FeCp in the single droplet. Namely, since the surface area/volume (A/V) ratio of a droplet increases with decreasing d , the above mentioned results can be reasonably understood by the fact that the rate of electron transfer from Fe(III) to FeCp at the interface becomes faster with the decrease in d .

The diameter-independent rate constant of the electron transfer (k_2') can be obtained by the relation $k_2 = (A/V)k_2'$. This relation indicates that observed k_2 should be linearly proportional to d^{-1} (i.e., $k_2 = (6/d)k_2'$), and the slope of the k_2 vs. d^{-1} plot corresponds to the rate constant per unit area; k_2' . Actually, the plot gave the fairly good linear relationship, and we determined k_2' to be $2.0 \times 10^{-2} \text{ M}^{-1}\text{cm}^{-1}\text{s}^{-1}$. Quite recently, the electron transfer rate constant at the macroscopic liquid/liquid interface was reported to be $0.01 \sim 1 \text{ M}^{-1}\text{cm}^{-1}\text{s}^{-1}$ (ref. 14), which was in good agreement with k_2' determined for the single droplet. The laser trapping - spectroscopy - electrochemistry method shows great potential for studying electron transfer reactions in emulsions.

MASS TRANSFER ACROSS THE MICRODROPLET/WATER INTERFACE

Mass transfer of a solute from the water phase to a single oil droplet was also studied by the laser trapping - spectroscopy - electrochemistry method. We report the electrochemically-induced dye formation reaction in a single droplet as a model of a photographic emulsion (ref. 15, 16). An oil-in-water emulsion was prepared by mixing a dibutyl phthalate (DBP; 1.17 g) solution of a phenol derivative (Cp; 30 mM) with an aqueous solution of gelatin (12.5 wt %; 4.68 g) and sodium dodecylsulfate (5 wt %; 1.17 g). The emulsion (0.10 g) was redispersed in a K_2CO_3 (0.40 M)/ KHCO_3 (0.32 M) buffer solution (pH = 10; 9.90 g) containing 4-N,N-diethyl-2-methylphenylenediamine (PPD; 5.0 mM) and Na_2SO_3 (20 mM), and KCl (0.10 M). A single DBP droplet was laser-trapped under the optical microscope and positioned near an Au microelectrode (9 μm wide, 100 μm long, $\sim 0.3 \mu\text{m}$ thickness). In the presence of OH^- (pH = 10) and Na_2SO_3 in the water phase, 4-N,N-diethyl-2-methylquinonediimine (QDI) produced by oxidation of PPD at the electrode (100 mV vs. Ag/AgCl) undergoes deamination by OH^- and/or sulfonation by SO_3^{2-} . On the other hand, if QDI diffuses to the droplet/water interface and reacts with Cp, the cyan dye (C-dye) is produced in the droplet as illustrated in Fig. 4 (ref. 15). This implies that the C-dye formation in the droplet is strongly dependent on the lifetime (τ) of QDI, since the dye formation competes with the deamination and/or sulfonation reactions in water. It has been reported that the deamination and sulfonation rates of QDI are $\sim 0.2 \text{ s}^{-1}$ and $\sim 2 \times 10^4 \text{ M}^{-1}\text{s}^{-1}$ at pH = 10, respectively. Under the present conditions of $[\text{SO}_3^{2-}] = 2 \times 10^{-2} \text{ M}$, therefore, τ of QDI in the water phase is mainly governed by the sulfonation reaction and is estimated to be $\sim 3 \text{ ms}$, which corresponds to the diffusion length of QDI (Δ) being $\sim 2 \mu\text{m}$ as calculated by the equation; $\Delta = (2D\tau)^{1/2}$, where $D \sim 5 \times 10^{-6} \text{ cm}^2\text{s}^{-1}$ for PPD was used for the calculation. The D value and the above discussion indicate that the C-dye formation is expected to be controlled by the distance between the droplet and the electrode in micrometer dimension.

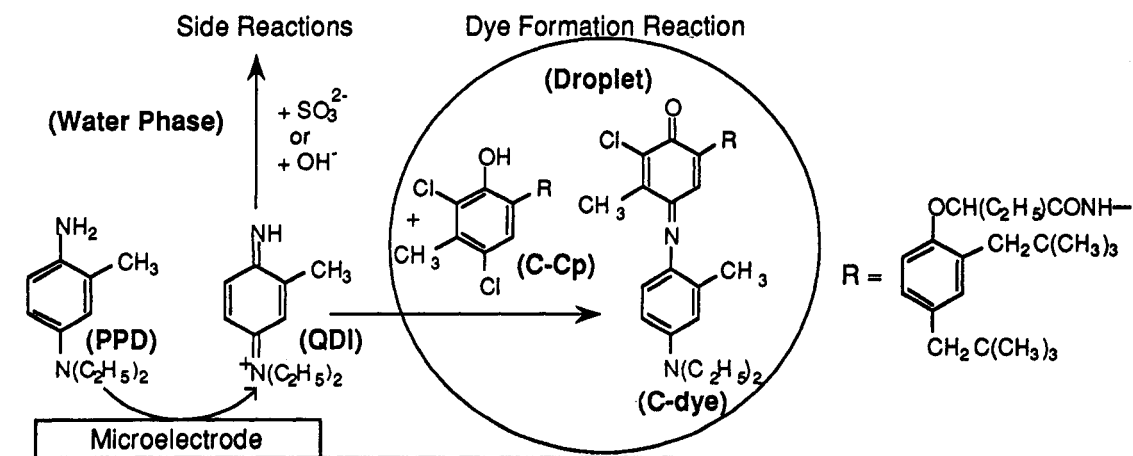


Fig. 4. Schematic illustration of the electrochemically induced dye formation reaction in a single droplet.

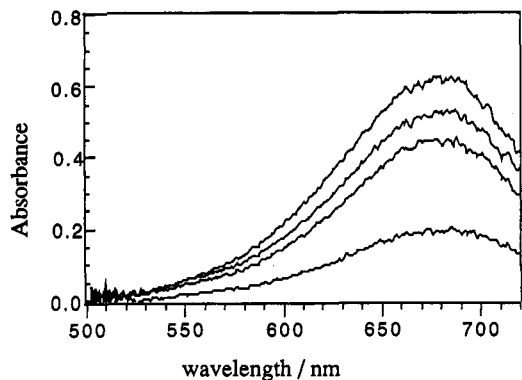


Fig. 5. Absorption spectra of a single laser-trapped droplet ($d = 10 \mu\text{m}$) during electrolysis ($t = 15, 30, 45,$ and 120 s) of PPD in the water phase.

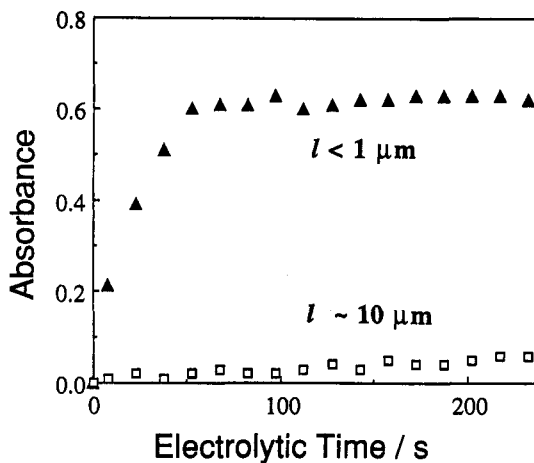


Fig. 6. Time conversion profile of the C-dye formation in a single-laser trapped droplet ($d = 10 \mu\text{m}$) positioned at $l < 1$ or $\sim 10 \mu\text{m}$.

When the edge-to-edge distance between the droplet and the electrode (l) is set $< 1 \mu\text{m}$ and the oxidation of PPD in the water phase is induced at the microelectrode, the efficient C-dye formation in the droplet can be observed as revealed from in situ measurements of the absorption spectrum of the droplet. Figures 5 and 6 demonstrate that the absorbance at 670 nm relevant to C-dye in the droplet increases with an electrolytic time (t) and almost levels off at $t > 150 \text{ s}$. On the basis of the absorbance at $t > 150 \text{ s}$, the molar extinction coefficient ($\epsilon_{670} = 2.8 \times 10^4 \text{ M}^{-1}\text{cm}^{-1}$), and the droplet diameter ($d = 10 \mu\text{m}$; optical path length), the dye formation yield in the single droplet was determined to be $\sim 70 \%$. The time course of the absorbance change was also analyzed for quantitative discussion on the dye formation reaction. As shown in Fig. 6, the absorbance of C-dye in the droplet increased single-exponentially. Since the concentration of QDI produced at the microelectrode is assumed to be almost constant ($\sim 5 \text{ mM}$) at $t > 5 \text{ s}$ owing to cylindrical diffusion of PPD to the microelectrode, the time conversion curve in Fig. 6 was analyzed as a pseudo-first-order reaction. The rate constant of the dye formation reaction between QDI and Cp in the droplet (k_{cp}) was thus calculated to be $8 \text{ M}^{-1}\text{s}^{-1}$ (ref. 16). However, the value is much smaller than that ($\sim 1 \times 10^3 \text{ M}^{-1}\text{s}^{-1}$) determined for the droplets (average $d \sim 0.1 \mu\text{m}$) in analogous photographic emulsions by a rotating ring-disk electrode method. In the Cp/QDI system, the dye formation reaction has been suggested to proceed at the oil-droplet/water interface, so that the coupling rate between QDI and Cp should be discussed based on the rate per unit droplet/water interfacial area, $k_{cp}' = (V/A)k_{cp}$, as in the case for the discussion in the preceding section. The k_{cp}' values determined for the single ($d = 10 \mu\text{m}$) and a number of the droplet ($d \sim 0.1 \mu\text{m}$) were calculated to be 1×10^{-3} and $\sim 2 \times 10^{-3} \text{ M}^{-1}\text{cms}^{-1}$, respectively. k_{cp}' obtained for the single droplet is comparable with that determined for a large number of the droplets by the rotating ring-disk electrode method. The rate constant of the dye formation reaction across the droplet/water interface was determined for the first time. Also, the present study proved that the coupling reaction between QDI and Cp took place at the droplet/water interface. Analogous experiments were performed for the droplets with various separations (l) from the electrode. The lifetime of QDI is limited to $\sim 2 \mu\text{m}$ under the present conditions as described above, so that the dye formation rate is expected to decrease with increasing l . Indeed, we confirmed that the dye formation reaction scarcely proceeded when the droplet was positioned at $l \sim 10 \mu\text{m}$ (Fig. 6). The present study showed a possibility for control of reactions in the droplet by the electrode - droplet distance in micrometer dimension.

CONCLUDING REMARKS

The microchemical technique of optical trapping - spectroscopy - electrochemistry has been shown to be a powerful means to investigate chemical reactions in small volumes, particularly in individual microdroplets and microparticles dispersed in solution. Flow cytometry has been frequently used for spectroscopic analyses of microparticles. However, the method cannot necessarily guarantee a single-particle measurement and also, a particle to be analyzed cannot be selected or monitored during experiments. Therefore, the method limits direct observation of chemical processes across the particle/solution boundary. The optical trapping-based methods are certainly superior to flow cytometry in respect to precise analyses of arbitrary microparticles as well as of interfacial phenomena in emulsions. As demonstrated in the present article, furthermore, the surface area/volume ratio increases with decreasing the diameter of a particle, so that various phenomena proceeding across the particle/solution boundary are expected to be controlled in micrometer dimension. Actually, the dye formation reaction in a single droplet was shown to be controlled by the distance between the droplet and the electrode. The very small mole number of a solute involved in micrometer dimension is also very advantageous to generate nonequilibrium states by a photochemical or electrochemical perturbation, which provides a new methodology for studying chemical mechanisms. A study on chemistry in single microparticles or in small volumes will be advanced based on using the potential of the optical trapping - spectroscopy - electrochemistry method, and further studies are now in progress in this laboratory.

ACKNOWLEDGMENT

The authors are greatly indebted to Messrs. K. Chikama and T. Suto for their intimate collaborations and discussions. N. K. also thanks to the Sumitomo Science Foundation for support of the research.

REFERENCES

1. H. Masuhara, *Pure Appl. Chem.*, **64**, 1279 (1992).
2. H. Masuhara, F. C. De Schryver, N. Kitamura, N. Tamai, Ed., *Microchemistry - Spectroscopy and Chemistry in Small Domains*, Elsevier, Amsterdam (1994).
3. K. Sasaki, M. Koshioka, H. Masuhara, *Appl. Spectro.*, **45**, 1041 (1991).
4. N. Tamai, T. Asahi, H. Masuhara, *Rev. Sci. Instrum.*, **64**, 2496 (1993).
5. M. Koshioka, H. Misawa, K. Sasaki, N. Kitamura, H. Masuhara, *J. Phys. Chem.*, **96**, 2909 (1992).
6. K. Nakatani, H. Misawa, K. Sasaki, N. Kitamura, H. Masuhara, *J. Phys. Chem.*, **97**, 1701 (1993).
7. T. Uchida, H. Sugimura, A. Sekiguchi, N. Kitamura, N. Shimo, H. Masuhara, *J. Electroanal. Chem.*, **351**, 343 (1993).
8. H. Misawa, M. Koshioka, K. Sasaki, N. Kitamura, H. Masuhara, *J. Appl. Phys.*, **70**, 3829 (1991).
9. H. Misawa, N. Kitamura, H. Masuhara, *J. Am. Chem. Soc.*, **113**, 7859 (1991).
10. K. Sasaki, H. Misawa, *Microchemistry - Spectroscopy and Chemistry in Small Domains*, p. 23, Elsevier, Amsterdam (1994).
11. A. Ashkin, *Phys. Rev. Lett.*, **24**, 156 (1970).
12. K. Sasaki, M. Koshioka, H. Misawa, N. Kitamura, H. Masuhara, *Appl. Phys. Lett.*, **60**, 807 (1992).
13. K. Nakatani, K. Chikama, H.-B. Kim, N. Kitamura, *Chem. Lett.*, 793 (1994).
14. R. A. Marcus, *J. Phys. Chem.*, **94**, 4152 (1990) and **95**, 2120 (1991).
15. K. Nakatani, T. Uchida, S. Funakura, A. Sekiguchi, H. Misawa, N. Kitamura, H. Masuhara, *Chem. Lett.*, 717 (1993).
16. K. Nakatani, T. Suto, M. Wakabayashi, H.-B. Kim, N. Kitamura, submitted.